# Infrared Galaxies in the Nearby Universe *

Jian-Ling Wang

1 National Astronomical Observatories, Chinese Academy of Sciences, Beijing 100012, China;
  *wjianl@bao.ac.cn*
2 Graduate School of Chinese Academy of Sciences, Beijing 100049, China

**Abstract**  We used the Sloan Digital Sky Survey (SDSS) Data Release 5 (DR5) to study the morphological properties of 1137 nearby infrared (IR) galaxies, most of which are brighter than 15.9 mag in $r$-band. This sample was drawn from a cross-correlation of the Infra-Red Astronomical Satellite (*IRAS*) point source catalog redshift survey with DR5 at $z \lesssim 0.08$. Based on this IR galaxy sample, we constructed five volume-limited sub-samples with IR luminosity ranging from $10^{9.5} L_\odot$ to $10^{12} L_\odot$. By deriving the IR luminosity functions (LF) for different morphological types, we found that normal spiral galaxies are the dominant population below $L_{\rm IR} \sim 8 \times 10^{10} L_\odot$; while the fraction of barred spiral galaxies increases with increasing IR luminosity and becomes dominant in spiral galaxies beyond $L_{\rm IR} \simeq 5 \times 10^{10} L_\odot$. As the IR luminosity decreases, the IR galaxies become more compact and have lower stellar masses. The analysis also shows that normal spiral galaxies give the dominant contribution to the total comoving IR energy density in the nearby universe, while, in contrast, the contribution from peculiar galaxies is only 39%.

**Key words:** galaxies: evolution — galaxies: interactions — galaxies: starburst — infrared: galaxies — galaxies: luminosity function

## 1 INTRODUCTION

Understanding how, when and where most stellar mass is produced is an important, unsolved problem. In the last decade, there have been numerous studies of star formation history as a function of redshift (e.g. Lilly et al. 1996; Madau et al. 1998). It has been confirmed by Spitzer observations that the star formation rate density has rapidly declined by a factor of $\sim 10$ since redshift $\sim 1$ (Le Floc'h et al. 2005). To understand the star formation process at high-redshift, it is a prerequisite to understand the properties of local star-forming galaxies.

The *IRAS* (Infra-Red Astronomical Satellite) database still plays an important role with data yet to be explored (Lonsdale et al. 2006; Wu et al. 1998a,b; Goto 2005; Pasquali et al. 2005; Cao et al. 2006; Wang et al. 2006). This all-sky survey conducted by *IRAS* produced two catalogs: the Faint Source Catalog (FSC, Moshir et al. 1992) and the brighter Point Source Catalog (PSC, Joint *IRAS* Science Working Group 1988). The Point Source Catalog Redshift survey (PSCz) obtained redshifts for all the sources in the PSC, which provides a unique catalog of IR galaxies in the nearby universe.

Based on *IRAS* redshift surveys, the IR luminosity function (LF) in the nearby universe has been well established (Soifer et al. 1987; Sanders & Mirabel 1996; Sanders et al. 2003). About 30% of the luminosity density is contributed from infrared emissions in 8–1000 $\mu$m (Soifer & Neugebauer 1991). On the other hand, although the luminous infrared galaxies (LIRGs: $L_{\rm IR} > 10^{11} L_\odot$) and ultraluminous infrared galaxies (ULIRGs: $L_{\rm IR} > 10^{12} L_\odot$) are rare and only account for $\sim 5\%$ of the total IR energy density in

nearby universe (Soifer & Neugebauer 1991; Kim & Sanders 1998; Le Floc'h et al. 2005), they are the dominant population responsible for the bulk of the comoving IR luminosity density at redshift beyond $z \sim 0.5$ (Le Floc'h et al. 2005; Pérez-González et al. 2005). While, at redshifts less than 0.5, a large fraction of the IR energy density is contributed by galaxies with $L_{IR} < 10^{11} L_\odot$. Given that there is a linear correlation between star formation rate (SFR) and IR luminosity (Kennicutt 1998), investigating the properties of galaxies with lower infrared luminosities will help to understand the star formation process. However, until now, there are few works on detail analysis of the IR LFs from different populations of local galaxies, especially for IR galaxies with different morphologies.

In this paper, we cross-correlate the PSCz catalog with the Sloan Digital Sky Survey (SDSS) Data Release 5 (DR5), and study the morphological properties of these star forming galaxies in detail. Our main goal is to derive the morphologically dependent IR LF, hence to know which type of galaxies is the dominant contributor to the comoving IR energy density in nearby universe. The structure of the paper is as follows. In Section 2, we describe how we cross-correlate the SDSS DR5 data with the PSCz data, and how we construct five volume-limited samples. In Section 3, we present and discuss the statistical results. In the final section, we summarize our results. Throughout this paper we use a cosmology with a matter density of $\Omega_{m,0} = 0.3$, a cosmological constant $\Omega_{\Lambda,0} = 0.7$ and a Hubble constant of $H_0 = 70 \, \mathrm{km \, s^{-1} \, Mpc^{-1}}$.

## 2 THE SAMPLE

Our IR galaxy sample is drawn from a cross-correlation of the PSCz catalogue with the SDSS DR5 photometric catalogue. PSCz is one of the *IRAS* redshift survey catalogues with 60 micron flux above 0.6 Jy. The catalogue has 15411 *IRAS* galaxies, of which 14677 objects have redshift available. The sample covers 84% of the sky and completes to $b_J < 19.5$ (Saunders et al. 2000). The SDSS DR5 photometric survey covers 7875 square degree[1], 215 million individual objects up to 22.2 mag at $g$- and $r$- band (Stoughton et al. 2002; Adelman-McCarthy et al. 2007). According to the calibration formula suggested by the 2dFGRS team[2], $g = b_J - 0.150 - 0.130(g - r)$, the faintest object in our volume-limited samples is $r \simeq 18.4$ mag (see the following) after Galactic extinction correction (Schlegel et al. 1998). Therefore, the SDSS DR5 photometric survey is deep enough to detect the vast majority of the optical counterparts of PSCz sources. When we perform the cross-identifications, all SDSS sources within $5''$ around the optical positions of PSCz are taken as the IR galaxy counterparts. When there are more than one SDSS source within the searching area, we choose the nearest one as the counterpart.

In order to test the robustness of this 2-dimensional (2D) cross-identifications, we also perform cross-correlation analysis between PSCz and the SDSS DR5 spectroscopic sample within $5''$ radius. Only 5% of our 2D matched sample galaxies have redshift differences larger than 3%. On the other hand, as our sample galaxies are nearby object, most our volume-limited sample galaxies ($\sim 98\%$) have sizes (three times half-light Petrosian radius) larger than $5''$, with median size $\sim 18''$, which is comparable to the typical position uncertainty of *IRAS* PSC. Therefore, our identification should be reliable. The cross-correlation yielded 3284 objects.

For each object, we estimate the total IR luminosity by the formula

$$L_{IR}(8 - 1000 \, \mu m) \approx 2 L_{60 \mu m}, \tag{1}$$

where the monochromatic luminosity, $L_{60 \mu m} = \nu L_{60 \mu m}$ (Lawrence et al. 1989; Bushouse et al. 2002; Arribas et al. 2004). This IR luminosity estimation is consistent with that from the more widely used formula (Hopkins et al. 2003) that uses both the 60 and 100 $\mu m$ fluxes.

Figure 1 shows the IR luminosity vs. redshift for all 3284 identified IR galaxies. The lower envelope is due to the IR flux limit of 0.6 Jy at $60 \, \mu m$. For the later statistical analysis, we further constructed five volume-limited sub-samples from the main sample (3284 galaxies) with IR luminosity ranges at $10^{9.5} L_\odot < L_{IR} < 10^{10} L_\odot$, $10^{10} L_\odot < L_{IR} < 10^{10.4} L_\odot$, $10^{10.4} L_\odot < L_{IR} < 10^{11} L_\odot$, $10^{11} L_\odot < L_{IR} < 10^{11.4} L_\odot$ and $10^{11.4} L_\odot < L_{IR} < 10^{12} L_\odot$, respectively. These sub-samples are marked as boxes in Figure 1. The

---

[1] The SDSS DR5 covers about 8000 deg$^2$ of sky which includes a small amount of imaging outside of the ellipse that defines the main-survey boundary, while the precise number for the photometric survey area is 7875 unique deg$^2$ (Adelman-McCarthy et al. 2007).

[2] *http://www.mso.anu.edu.au/2dFGRS/*
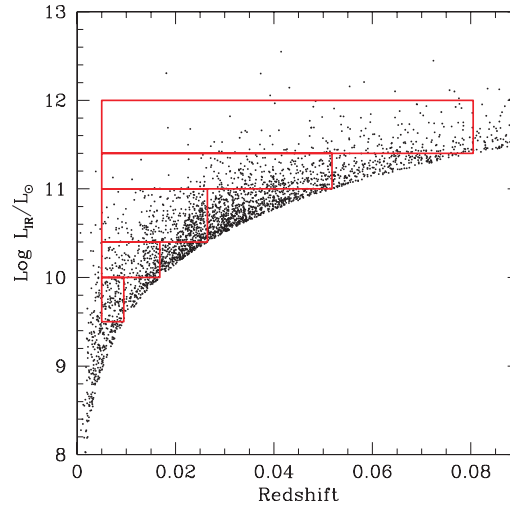
**Fig. 1** IR luminosity (estimated using Eq. (1)) vs. redshift. The five red boxes indicate, from top to bottom, our five IR volume-limited samples.

**Table 1** Morphological classification of IR galaxies in five IR luminosity bins and the CIRED contributed by different morphological types.

| Range of log $L_{IR}/L_\odot$ | 9.5~10 $0.005 \leq z < 0.0095$ | | 10~10.4 $0.005 \leq z < 0.0168$ | | 10.4~11 $0.005 \leq z < 0.0265$ | | 11~11.4 $0.005 \leq z < 0.0518$ | | 11.4~12 $0.005 \leq z < 0.0805$ | | 9.5~12 CIRED | |
|---|---|---|---|---|---|---|---|---|---|---|---|---|
| | $N$ | % | $N$ | % | $N$ | % | $N$ | % | $N$ | % | $N$ | % |
| Barred spiral | 8 | 8 | 23 | 13 | 65 | 17 | 50 | 17 | 20 | 11 | 166 | 14 |
| Nonbarred spiral | 28 | 28 | 37 | 21 | 63 | 16 | 19 | 6 | 3 | 2 | 150 | 18 |
| Highly-Inclined spiral | 45 | 45 | 56 | 32 | 96 | 25 | 40 | 14 | 3 | 2 | 240 | 28 |
| Peculiar | 18 | 18 | 57 | 33 | 159 | 42 | 187 | 63 | 157 | 86 | 578 | 39 |
| S0 | 2 | 2 | 1 | 1 | 0 | 0 | 0 | 0 | 0 | 0 | 3 | 1 |
| Total | 101 | 100 | 174 | 100 | 383 | 100 | 296 | 100 | 183 | 100 | 1137 | 100 |

redshift intervals and number of objects for each subsample are listed in Table 1. Note that the lower redshift cut in each subsample is to exclude redshifts that significantly deviated from the Hubble flow. Finally, there are 183, 296, 383, 174 and 101 objects in each volume-limited sub-samples from high to low IR luminosity bins (see Table 1). These 1137 IR galaxies comprising the five sub-samples will be our working sample. Figure 2 shows the number distributions of IR luminosity, redshift, and $r$-band magnitude for the sample galaxies. We can see that most of the galaxies ($\sim 90\%$) are brighter than 15.9 mag in the SDSS $r$ band, hence reliable morphological classifications can be made for most of the galaxies (Fukugita et al. 2004).

Note that there exists a well-known photometric problem in SDSS in that the big bright objects tend to be deblended into several smaller parts. So we visually checked all the color images against the position of identified source. There were 301 objects off the center of the galaxies or located in mistakenly deblended pieces (of big galaxies). In our analysis, we used the total luminosity of the big galaxies rather than each small, deblended part.

Figure 3 shows the SDSS survey sky coverage[3] on an Aitoff projection in Galactic coordinates. Also shown are the PSCz masked region affected by heavy contamination, as well as our five volume-limited samples. Using the mask file of PSCz and the SDSS sky survey coverage tables, we can calculate the SDSS survey region masked by PSCz. There is about $350 \deg^2$ masked by PSCz. So the total region covered by SDSS and PSCz is $7525 \deg^2$, corresponding to 18.2% of the whole sky. This number will be used to

---

[3] The SDSS sky survey coverage can be found in website: *http://www.sdss.org/dr5/coverage/index.html*. For details of the sky coverage tables please refer to SDSS website.
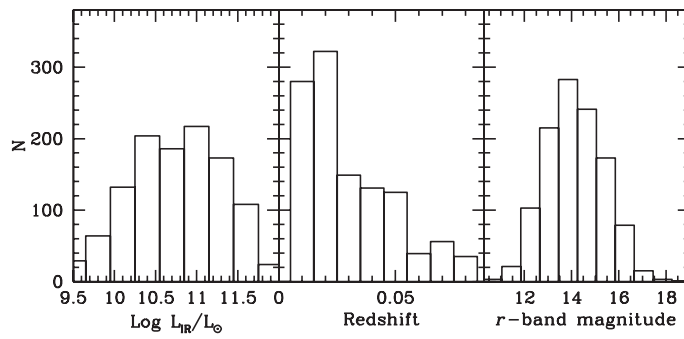
**Fig. 2** Number distributions of infrared luminosity, redshift and apparent magnitude for all five volume-limited samples.
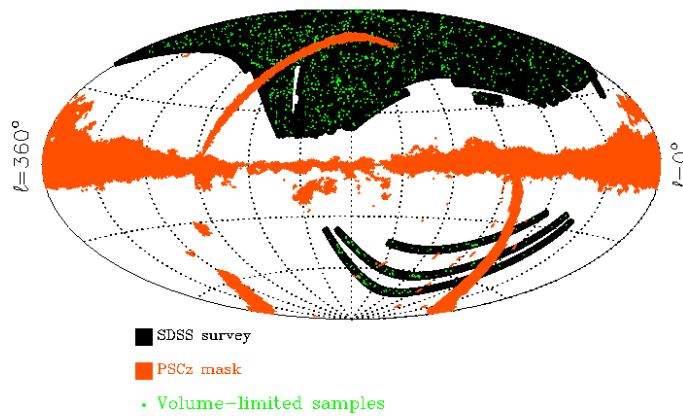


**Fig. 3** Aitoff projection in Galactic coordinates showing the SDSS DR5 survey coverage, the PSCz masked region, and our five volume-limited samples.

cross-check the normalization of our IR luminosity function. Using this sky coverage information, we can estimate how many PSCz sources are covered by the SDSS survey. It should be $15411 \times 7525/(41253 \times 0.84) \simeq 3347$. Disregarding the redshift completeness, the completeness for our cross-correlation is $3284/3347 \simeq 98\%$.

Note that there are 5% of PSCz galaxies without redshift data, which may affect the completeness of our samples. However, most of these PSCz galaxies are distributed around the Galactic plane with $|b| < 30\,^\circ$ (see fig. 4 of Saunders et al. 2000), while the SDSS survey covers the north pole region with a small fraction of the located in $|b| < 30°$ (see Fig. 3). Therefore, such incompleteness is trivial, which will be confirmed by the normalization of our LF.

## 3  ANALYSIS AND RESULTS

### 3.1  Morphological Classification

We visually examined all the $r$-band images for the morphological classifications. Then we used the color-images for the cross checks (see Wang et al. 2006). We classified all galaxies into three types: interacting/merging galaxies (or peculiars), elliptical/S0 galaxies and spirals (including barred, nonbarred and highly-inclined spirals).

We first picked out the peculiars that show interacting/merging signatures or merged relics. Then, the elliptical/S0 galaxies were selected from the remainder that either have symmetric structures and no apparent disk features (ellipticals) or show a lens-shape without any conspicuous structure in the disk (S0). The rest are all spirals. We further divided the spirals into barred, nonbarred and highly-inclined spirals based on isophote analysis as well as visual examination of the images. Spirals with inclination angle $i$ greater than $60°$ are defined as highly-inclined spirals (Abraham et al. 1999). The barred spirals are characterized by the rapid changes in the position angle and ellipticity with the radius (Jogee et al. 2004; Zheng et al. 2005; Menéndez-Delmestre et al. 2007). Note that for the highly-inclined spirals, it is difficult to see whether they are barred or not, and hence they are grouped into a separate category (highly-inclined spirals).

The number and fraction of each type of galaxies are listed in Table 1. Note that there are no ellipticals and only three S0 galaxies with low IR luminosities that show strong star forming activities, Balmer absorption features or an obvious nuclear dust lane. We assume these three S0 galaxies to be at a later stage of interaction/merger, and we will not do any special analysis on these.

## 3.2  Infrared Luminosity Function for Separate Morphological Types

The red and blue lines in Figure 4 show the infrared luminosity functions (IR LF), for the peculiars and spiral galaxies, respectively. The normalization of the IR LFs is obtained by equating the total IR energy over the range from $10^{9.5}L_⊙$ to $10^{12}L_⊙$ with that obtained by integrating the IR LF curve of Takeuchi et al. (2003). The sky coverage obtained from this method is 17.3%, which is more or less the same as the sky coverage of our sample (18.2%). We can see that the overall shape of IR LF for whole sample galaxies (yellow open circles) matches that of Takeuchi et al. (2003) (green line) very well.

It is clear from Figure 4 that, with increasing IR luminosity, the contribution to the IR LF by the normal spiral galaxies decreases, while that from the peculiars increases. Especially, the normal spirals are the dominant population below $L_{\mathrm{IR}} \sim 8 \times 10^{10} L_⊙$, while above $L_{\mathrm{IR}} \sim 8 \times 10^{10} L_⊙$ the peculiars are the dominant population.

Based on the IR LF, we estimated the comoving infrared energy density (CIRED) in the IR luminosity range from $10^{9.5}L_⊙$ to $10^{12}L_⊙$ contributed respectively by the normal spirals and the interacting/mergers. See Table 1. The peculiars contribute only 39% to CIRED in the nearby universe, thus, the infrared energy density in the local universe is mainly from normal spiral galaxies.

In order to assess the role of the bar in triggering star formation, we further investigated separately the IR LFs of barred and nonbarred spirals. Under the assumption that the fraction of barred and nonbarred spirals is independent of the inclination of the spiral, we partitioned all spirals irrespective of inclination barred and non-barred spirals and the separate IR LFs are shown in Figure 5. The nonbarred spirals are obviously the dominant population at IR luminosity below $\sim 5 \times 10^{10} L_⊙$, the barred spirals play increasingly greater role with increasing luminosity and become the dominate population when IR luminosity exceeds $\sim 5 \times 10^{10} L_⊙$.

The identification of the bar in this work is based on the optical images, which may suffer dust extinction, resulting in a lower rate of identification. To assess this effect, we used near-infrared images from Large Galaxy Atlas (LGA), assembled from 2MASS (Two Micron All-Sky Survey) with image size from $2'$ to $2°$ (Jarrett et al. 2003). The LGA includes over 500 large galaxies with individual and co-added $J$-, $H$-, and $Ks$- band images. The completed atlas provides the aggregate flux for each galaxy and a detailed view of the infrared morphology. We cross-correlated our sample IR galaxies with the LGA catalogue and found 30 objects in common, comprising 13 peculiars, 9 highly-inclined spirals and 8 low-inclination spirals. Six of the low-inclination spirals are bar-spirals from morphological classification based on the SDSS images. However, the $Ks$ band images of the eight low-inclination spirals show clearly that seven of these objects (rather than just six) are obvious barred spirals. This seems to indicate that the fraction of barred objects based on optical images could be underestimated.

## 3.3  The Contribution of IR Galaxies to Star Formation Activity

In order to know the contributions to comoving infrared energy density (CIRED) by different species of IR galaxies in the nearby universe, we investigate the dependence of CIRED on such parameters of the galaxies as concentration index ($R_{90}/R_{50}$), stellar mass, stellar surface mass density, half-light radius ($R_{50}$) and IR dust color.
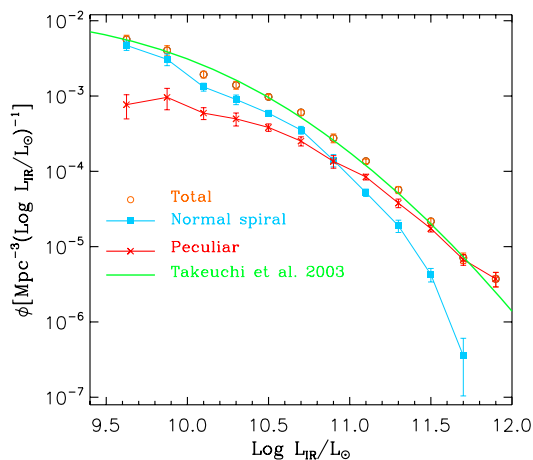
**Fig. 4** IR LF for separate morphological types. The red and blue lines are for interacting/merging galaxies and spiral galaxies, respectively. The yellow open circles for the whole sample, the green line is the analytic function of Takeuchi et al. (2003). The 1 $\sigma$ error bars from Poisson statistics are marked.
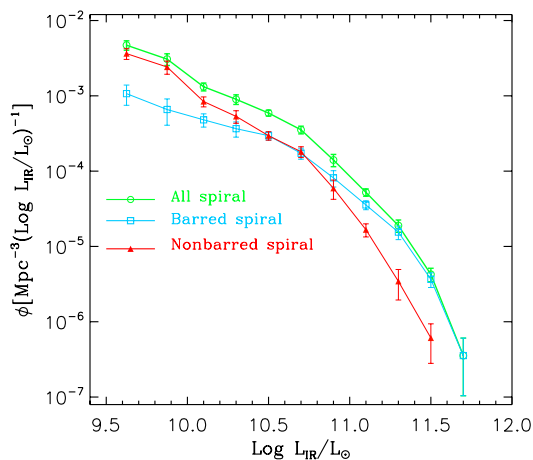


**Fig. 5** IR LF of spiral galaxies. The green line is for all spirals, red and blue lines are the IR LFs for nonbarred spirals and barred spirals, respectively. The 1 $\sigma$ error-bars from Poisson statistics are shown.

The concentration index is defined as the ratio of $C = R_{90}/R_{50}$, where $R_{90}$ and $R_{50}$ are the radii enclosing 90% and 50% of the Petrosian $r$-band luminosity, respectively. It is well known that there is a good correlation between the concentration parameter and the Hubble type: the early type galaxies tend to be more concentrated than the later type galaxies (Shimasaku et al. 2001; Strateva et al. 2001). For ellipticals with classic de Vaucouleurs profiles, $C$ is $\sim 5.5$, and for spirals with pure exponential profiles, $C$ is $\sim 2.3$. Strateva et al. (2001) proposed a cut at $C = 2.6$ to separate early- and late-type galaxies. From top-left panel of Figure 6, we can see that median value of concentration index $R_{90}/R_{50}$ is $\sim 2.4$ and about 63% of CIRED are contributed by galaxies with $R_{90}/R_{50} < 2.6$, indicating that the disk dominant spirals give the dominant contribution to the CIRED.
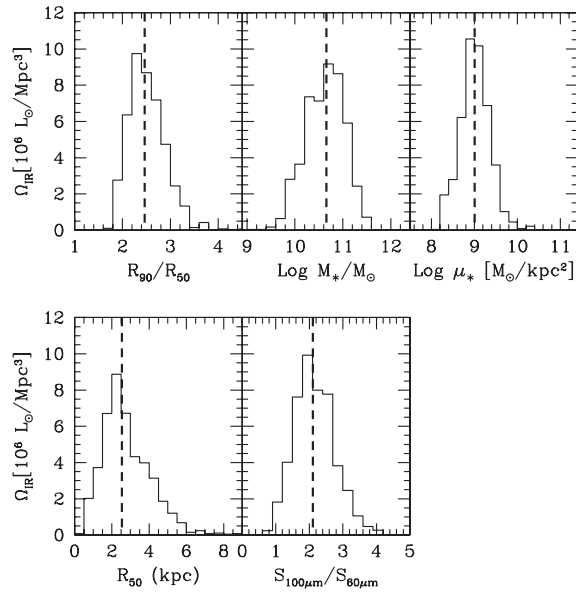
**Fig. 6** Comoving infrared energy density (CIRED) as functions of, respectively, the concentration index ($R_{90}/R_{50}$), stellar mass, surface mass density, Petrosian half-light radius ($R_{50}$) and IR color. The dashed-line in each panel marks the median value.

We estimate the old stellar mass for each object from the $g$-$r$ color and the $r$-band luminosity, following Bell et al. (2003). The photometric $k$-correction was calculated using the method of Blanton et al. (2007). The stellar surface mass density $\mu_*$ is defined as $M_*/(2\pi R_{50}^2)$. From top-middle and top-right panel of Figure 6, the galaxies with stellar mass ranging from $10^{10}$ $M_\odot$ to a few $\times$ $10^{11}$ $M_\odot$ and with surface mass density from few time $10^8$ $M_\odot$ kpc$^{-2}$ to a few times $10^9$ $M_\odot$ kpc$^{-2}$ give the main contribution to the CIRED. The bottom left panel of Figure 6 shows that most of the CIRED ($\sim 63\%$) is contributed from galaxies with half-light radii smaller than 3 kpc. Brinchmann et al. (2004) have investigated optically selected star forming galaxy properties using the SDSS data. They showed that the peak size contributing to stellar mass and star formation rate density is about 3 kpc (see their fig. 20). This indicates that in the nearby universe, most CIRED is contributed by compact galaxies and IR selected SF galaxies, rather than optical selected galaxies. Furthermore, Takeuchi et al. (2003) used the median value $S_{100\mu m}/S_{60\mu m} = 2.1$ in their sample to separate the warm dust from cool dust, which is almost the same as the median value of Helou (1986), 2.1 this value coincides with the median value in the bottom right panel of Figure 6. For our sample IR galaxies, this indicates that the galaxies with warm dust contribute one-half of the CIRED. Given that LIRGs dominant contributions to the CIRED at redshift ($z \sim 0.7$) and that LIRGs tend to be objects with warm dust (Soifer et al. 1987), we can expect that most of the CIRED at intermediate or high redshifts will be contributed by warmer dust. A direct comparison of the typical dust temperature of the CIRED contributor will help specifying the evolution of the dust.

In the top panel of Figure 7, we plot the stellar mass versus IR luminosity for spiral galaxies. It is clear that the IR luminosity decreases with decreasing stellar mass. The median values of stellar mass are, respectively, $1.2 \times 10^{11}$ $M_\odot$, $9.1 \times 10^{10}$ $M_\odot$, $6.6 \times 10^{10}$ $M_\odot$, $3.9 \times 10^{10}$ $M_\odot$ and $1.6 \times 10^{10}$ $M_\odot$, for the spirals in our five volume-limited samples. The bottom panel of Figure 7 shows $R_{50}$ versus the IR luminosity for the spiral galaxies, here $R_{50}$ is the Petrosian half-light radius. There is also a trend that as the size decreases, the IR luminosity decreases.

Therefore, it is clear that the massive and larger galaxies could have stronger infrared emissions: this is consistent with the statement of Heckman (2005) that SFR is correlated with the velocity dispersion of the galaxies, and the smaller systems are less able to host violent star formation activities like the LIRGs or ULIRGs.
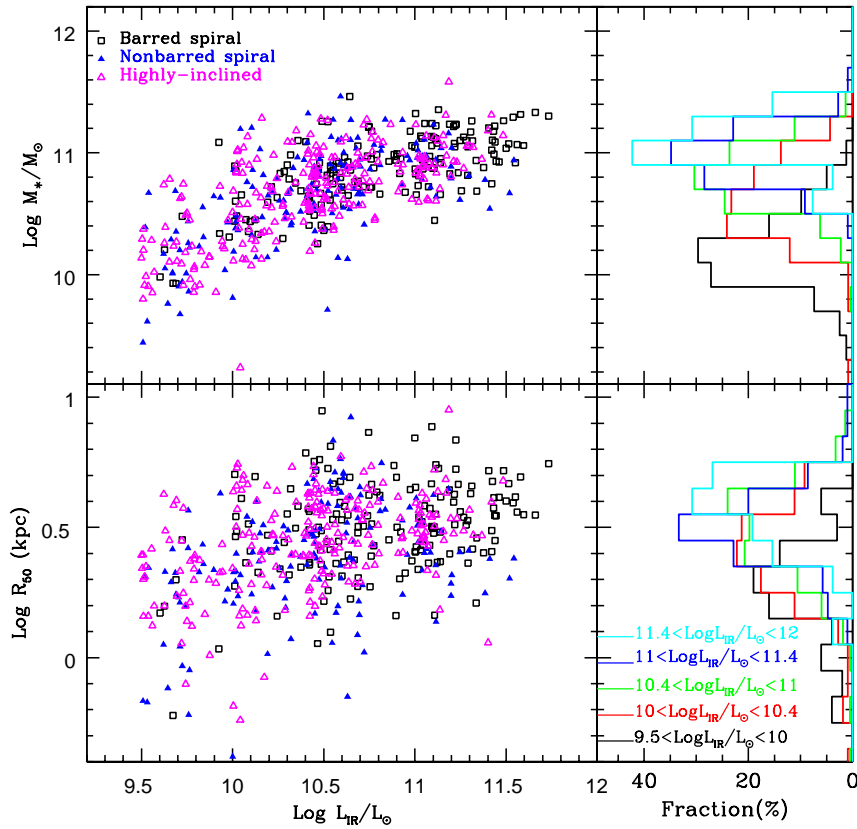
**Fig. 7** Stellar mass and $R_{50}$ as functions of IR luminosity. The histograms on the right show the distributions of stellar mass and $R_{50}$ for the five volume-limited samples.

## 4 CONCLUSIONS

In this paper, we studied properties of 1137 IR galaxies based on their SDSS photometric data drawn from a cross-correlation of the *IRAS* point source catalog redshift survey with the SDSS DR5 at $z \lesssim 0.08$. Especially, we constructed five volume-limited samples with IR luminosity ranging from $10^{9.5} L_\odot$ to $10^{12} L_\odot$ to derive the infrared luminosity function for different morphological types in nearby universe [4].

Our main conclusions are as follows:

– With increasing IR luminosity, the contribution of interacting/merging galaxies to the IR LF increases, while the contribution by normal spiral galaxies decreases. The normal spiral galaxies are the dominant population below $L_{\rm IR} \sim 8 \times 10^{10} L_\odot$, but above $L_{\rm IR} \sim 8 \times 10^{10} L_\odot$ the dominance passes to the interacting/merging galaxies. This means that interaction/merger is the most effective mechanism to trigger violent star forming activities in the nearby universe.

– Nonbarred spirals are obviously the dominant population at IR luminosities below $\sim 5 \times 10^{10} L_\odot$, while barred spirals play the more important role for the IR LF at higher luminosities, and become the dom-

---

[4] Note that our study complements that of Goto (2005) who studied the optical properties of 4248 *IRAS* galaxies selected from the faint source catalogue of *IRAS*. Although Goto (2005) did not consider the morphological types of the galaxies, he obtained the conclusion that as the IR luminosity decreases, the fraction of mergers decreases, while that of normal spiral galaxies increases. This is consistent with our results.

inate population when the IR luminosity exceeds $\sim 5 \times 10^{10} L_{\odot}$. This implies that bar instability is an important mechanism to transport the gas and to trigger star forming activities.

– The normal spiral galaxies provide the dominant contribution to the total comoving IR energy density in the nearby universe, while the contribution from interacting/merging galaxies is only 39%.

– With decreasing IR luminosity, the stellar mass and the size of the galaxy also decrease. Low IR luminosity galaxies have on average small stellar masses and more compact sizes, at least in the IR luminosity range between $10^{9.5} L_{\odot}$ to $10^{12} L_{\odot}$, while high IR luminosity galaxies tend to be larger systems with higher stellar masses and larger sizes.

Our study of nearby IR galaxies is relevant to their high redshift counterparts, which are the dominate contributor of cosmic SFR density and cosmic IR background (Le Floc'h et al. 2005). The current results provide a good analog for the investigations of high redshift star forming galaxies.

## References

Adelman-McCarthy J. K., Agüeros M. A., Allam S. S. et al., 2007, ApJS, 172, 634
Arribas S., Bushouse H., Lucas R. A. et al., 2004, AJ, 127, 2522
Bell E. F., McIntosh D. H., Katz N., Weinberg M. D., 2003, ApJS, 149, 289
Blanton M. R., Roweis S., 2007, AJ, 133, 734
Brinchmann J., Charlot S., White S. D. M. et al., 2004, MNRAS, 351, 1151
Bushouse H. A., Borne K. D., Colina L. et al., 2002, ApJS, 138, 1
Cao C., Wu H., Wang J. L. et al., 2006, Chin. J. Astron. Astrophys. (ChJAA), 6, 197
Fukugita M., Nakamura O., Turner E. L. et al., 2004, ApJ, 601, L127
Goto T., 2005, MNRAS, 360, 322
Heckman T. M., 2005, astro-ph/0502022
Helou G., 1986, ApJ, 311, L33
Jarrett T. H., Chester T., Cutri R. et al., 2003, AJ, 125, 52
Jogee S., Barazza F. D., Rix H. W. et al., 2004, ApJ, 615, L105
Joint IRAS Science Working Group. 1988. IRAS Catalogs and Atlases: The Point Source Catalog, Version 2.0 (NASA RP-1190) (Washington, DC: GPO) (PSC)
Kennicutt R. C., 1998, ARA&A, 36, 189
Kim D.-C., Sanders D. B., 1998, ApJS, 119, 41
Lawrence A., Rowan-Robinson M., Leech K. J. et al., 1989, MNRAS, 240, 329
Le Floc'h E., Papovich C., Dole H. et al., 2005, ApJ, 632, 169
Lonsdale C. J., Farrah D., Smith H. E., 2006, Astrophysics Update 2, 285

Lilly S. J., Le Fevre O., Hammer F. et al., 1996, ApJ, 460, L1

Madau P., Pozzetti L., Dickinson M., 1998, ApJ, 498, 106

Menéndez-Delmestre K., Sheth K., Schinnerer E. et al., 2007, ApJ, 657, 790

Moshir M., Kopan G., Conrow J. et al., 1992. Explanatory Supplement to the *IRAS* Faint Source Survey, Version 2, JPL
  D-10015 8/92, Pasadena: JPL

Hopkins A. M., Miller C. J., Nichol R. C. et al., 2003, ApJ, 599, 971

Pasquali A., Kauffmann G., Heckman T., 2005, MNRAS, 361, 1121

Pérez-González P. G., Rieke G. H., Egami E. et al., 2005, ApJ, 630, 82

Sanders D. B., Mazzarella J. M., Kim D.-C. et al., 2003, AJ, 126, 1607

Sanders D. B., Mirabel I. F., 1996, ARA&A, 34, 749

Saunders W., Sutherland W. J., Maddox S. J. et al., 2000, MNRAS, 317, 55

Soifer B. T., Neugebauer G., 1991, AJ, 101, 354

Soifer B. T., Sanders D. B., Madore B. F. et al., 1987, ApJ, 320, 238

Schlegel D. J., Finkbeiner D. P., Davis M., 1998, ApJ, 500, 525

Shimasaku K., Fukugita M., Doi M. et al., 2001, AJ, 122, 1238

Stoughton C., Lupton R. H., Bernardi M. et al., 2002, AJ, 123, 485

Strateva I., Željko I., Knapp G. R. et al., 2001, AJ, 122, 1861

Takeuchi T., Yoshikawa K., Ishii T. T., 2003, ApJ, 587, L89

Wang J. L., Xia X. Y., Mao S. et al., ApJ, 649, 722

Wu H., Zou Z. L., Xia X. Y. et al., 1998a, A&AS, 127, 521

Wu H., Zou Z. L., Xia X. Y. et al., 1998b, A&AS, 132, 181

Zheng X. Z., Hammer F., Flores H. et al., 2005, A&A, 435, 507